# Seasonal Redistribution and Conservation of Atmospheric Mass in a General Circulation Model

HUUG M. VAN DEN DOOL

*Climate Analysis Center, National Meteorological Center, Washington, D.C.*

SURANJANA SAHA

*Development Division, National Meteorological Center, Washington, D.C.*

(Manuscript received 18 May 1991, in final form 7 April 1992)

ABSTRACT

A 10-year run was made with a reduced resolution (T40) version of NMC's medium-range forecast model. The 12 monthly mean *surface* pressure fields averaged over 10 years are used to study the climatological seasonal redistribution of mass associated with the annual cycle in heating in the model. The vertically integrated divergent mass flux required to account for the surface pressure changes is presented in 2D vector form. The primary outcome is a picture of mass flowing between land and sea on planetary scales. The divergent mass fluxes are small in the Southern Hemisphere and tropics but larger in the midlatitudes of the Northern Hemisphere, although, when expressed as a velocity, nowhere larger than a few millimeters per second. Although derived from a model, the results are interesting because we have described aspects of the global monsoon system that are very difficult to determine from observations.

Two additional features are discussed, one physical, the other due to postprocessing. First, we show that the local imbalance between the mass of precipitation and evaporation implies a divergent water mass flux that is large in the aforementioned context (i.e., cm $s^{-1}$). Omission of surface pressure tendencies due to the imbalance of evaporation and precipitation (order 10–30 mb per month) may therefore be a serious obstacle in the correct simulation of the annual cycle. Within the context of the model world it is also shown that the common conversion from *surface* to *sea level* pressure creates very large errors in the mass budget over land. In some areas the annual cycles of surface and sea level pressure are 180° out of phase.

## 1. Introduction

The definition of monsoons involves the seasonal reversal of otherwise very persistent near-surface winds (Ramage 1971; Lamb 1972). A related result of the seasonal variation in heating and horizontal heating gradients is the rearrangement of mass in the atmosphere. The latter has understandably not become the working definition of monsoons because 1) surface winds can be felt by humans while pressure cannot, and 2) after measuring systems became available it was concluded that pressure differences in the tropics are often not accurately known.

At the National Meteorological Center (NMC) a 10-year run was made with the operational (as of fall 1990) medium-range forecast (MRF) model, albeit at reduced resolution, that is, truncated triangularly at zonal wavenumber 40 instead of 80. The model has 18 vertical levels in sigma coordinates. All external conditions (solar radiation, sea ice, sea surface temperature, soil moisture, and snow depth and cover) were prescribed to evolve according to their climatological annual cycle. Although this model does not substitute for reality, it does provide an internally consistent and complete dataset. In this spirit we present the seasonal variation of the vertically integrated mass in the model (i.e., the surface pressure $p_*$) and the attendant divergent mass flux required to explain the $p_*$ changes that occur seasonally. A picture emerges of mass flowing from land to ocean (and back about 6 months later) and from one hemisphere to the other orchestrated by solar radiation.

The seasonal redistribution of mass is of special interest because it can be determined from observations only with great difficulty. Divergent mass fluxes are equivalent to winds on the order of millimeters per second. This is too small to be measured directly. Ignoring several complications due to water vapor and its mass sources and sinks, it would be possible to derive the divergent mass flux from observed seasonal changes in $p_*$, which are accurately known where measured. Gordon (1953) alludes to this possibility, but except for some work pertaining to the zonal mean meridional mass flux (Oort 1983; Trenberth et al. 1987), we are

*Corresponding author address:* Dr. Huug M. van den Dool, Prediction Branch, Climate Analysis Center, National Meteorological Center, Washington, DC 20233.

not aware of publications describing such attempts. (A. H. Oort kindly shared with us an unpublished manuscript by J.-P. Huot on the 2D divergent mass flux associated with the seasonal cycle in observed $p_*$.)

At this point it is important to distinguish *sea level* from *surface* pressure. The latter is measured, but the former is more commonly made available and studied. The annual cycle in sea level pressure (Gordon 1953; Hsu and Wallace 1976; Trenberth 1981) has been known for a long time but can be quite misleading when interpreted in terms of the local or global mass budget. By necessity, mass is created or destroyed by the usual surface to sea level pressure conversion (Trenberth 1981; Trenberth et al. 1987).

The seasonal redistribution of mass and the seasonally changing monsoon winds are linked, of course. The $p_*$ field largely determines the near-surface winds, even at low latitudes (Murphree and Van den Dool 1988). The changes in $p_*$, however, are brought about by the vertically integrated divergent mass flux. We will display the latter, and it should be kept in mind that although the low-level winds transport enough air to change $p_*$ by much more than is observed (Boer 1986), they may not seem related to $\partial p_*/\partial t$ because of compensation aloft.

This paper is devoted to the diagnosis of model output, although some comparison with observations will be made in the discussion. One of the several difficulties in comparing with observations is the variable role of water vapor in nature. In the NMC model the hydrostatic mass is not changed when evaporation takes place (or when rain is falling); only the virtual temperature is changed. This is physically incorrect; that is, dry mass should be conserved, not total mass. The present dataset allows us to show that this is a serious inconsistency if one tries to simulate the annual cycle. A change in the continuity equations appears to be called for.

## 2. Data and analysis

The only model output fields used in this study are 10-year mean surface pressure fields for each calendar month given on a regular latitude–longitude grid of 2.5° × 2.5°. One minor correction had to be applied to each of the 12 maps. For numerical reasons the global-mean mass is not precisely conserved, but increased by 2.5 mb over 10 years. We therefore made the global mean $p_*$ in each of the 12 months equal to the global and annual mean $p_*$, a space-independent correction of less than 0.1 millibar.

As pointed out by Oort (1983), it makes little sense to display maps of $p_*$ itself because they mostly reflect the height of the terrain (spatial variations of a few hundred millibars). To bring out the dynamically interesting temporal variation (order 10 mb), some subtraction has to be made to eliminate the orography. Figure 1 (described in section 3) shows for each of the midseason months a map of the deviation from the annual mean, that is, $p_* - \bar{\bar{p}}_*$, where the double bar refers to a *local* annual mean.

The vertically integrated divergent mass flux $\mathbb{M}$, given in Fig. 2 for April and October, is calculated from

$$g\nabla \cdot \mathbb{M} = -\frac{\partial p_*}{\partial t}, \tag{1}$$

where $g$ is the acceleration of gravity. The rhs in (1) for April (for instance) is determined from the two-month centered difference between May and March. Equation (1) is solved by using spherical harmonics and yields only the divergent mass flux—we do not consider the rotational mass flux. The unit of mass flux is kg m$^{-1}$ s$^{-1}$ but has been transformed into a wind by realizing that

$$g\nabla \cdot \mathbb{M} = \nabla \cdot \int_0^{p_*} \mathbf{V} dp \tag{2}$$

$$= \nabla \cdot p_* \langle \mathbf{V} \rangle, \tag{2a}$$

where $\mathbf{V}$ is the divergent wind and $\langle \mathbf{V} \rangle$ represents the vertically averaged wind. One can see that

$$\langle \mathbf{V} \rangle = g\mathbb{M}/p_*. \tag{3}$$

Equation (3) is not strictly valid (it would only be if $p_*$ were constant in space) but is used here just to express a mass flux in terms of a wind.

In summary, the mass flux (2D vector) is calculated according to (1) but displayed as a velocity in units of millimeters per second using (3). Because we have a consistent dataset we could have, alternatively, calculated $\mathbf{M}$ from (2) using 18 levels of wind data to arrive at the same result.

## 3. Results

### a. Pressure anomalies

In Fig. 1 we show four midseason monthly maps of $p_* - \bar{\bar{p}}_*$, hereafter referred to as anomalies, that is, the surface pressure surplus/deficit relative to the annual mean. Contours are every 5 mb for January and July and 2.5 mb for April and October, and negative anomalies are shaded. There are two major features in the annual cycle of these anomalies. One is primarily in the Northern Hemisphere (NH), the second in the tropics and Southern Hemisphere (SH).

We start with the latter in February/March. At this time there is a well-defined zonally symmetric negative anomaly of a few millibars at and south of the equator, straddled by likewise zonally symmetric but positive anomalies in the SH all the way to the pole, and in the NH up to 30°N. This configuration weakens and breaks up in April and May and reverses sign by July/August. The next seasonal reversal begins in October and is completed mostly by January. While the amplitude of

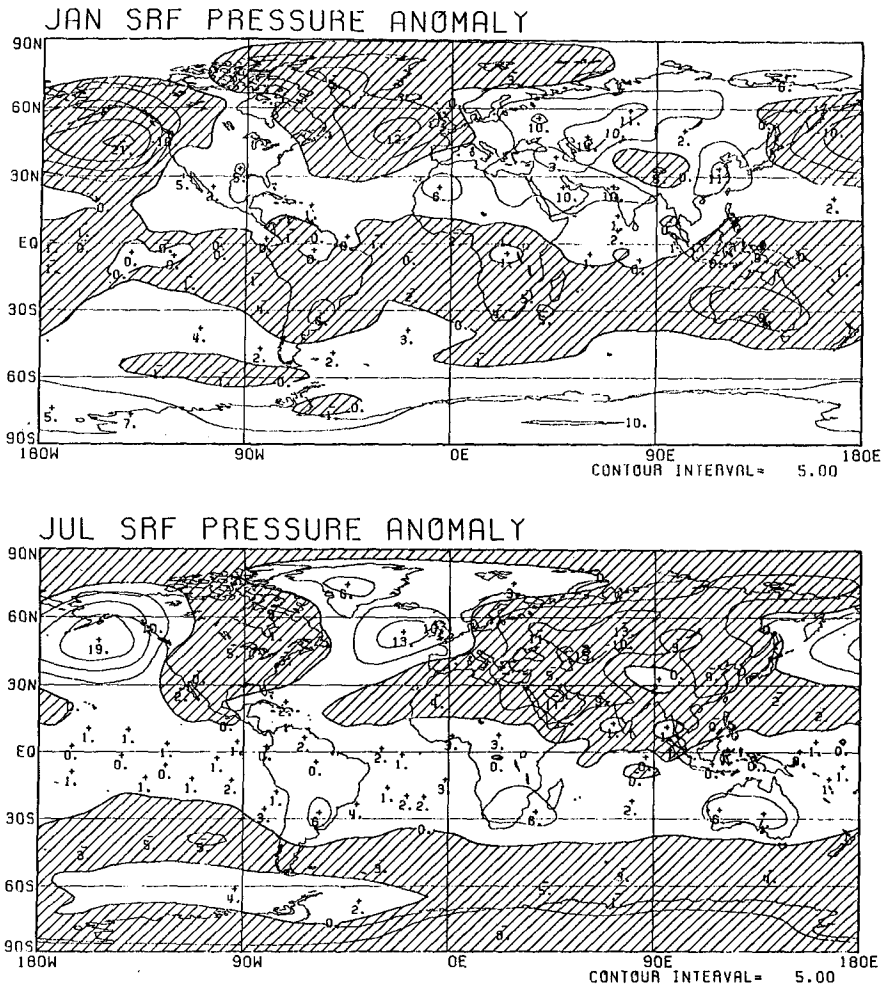


FIG. 1. Departure of surface pressure from its local annual mean in four panels, one for each of the midseason months. Units are in millibars; contours every 5 mb in January and July, and every 2.5 mb in April and October; negative values are shaded.

this oscillation is just a few millibars, the very large zonal scale is impressive.

The second major feature is mostly north of 30°N and involves in particular the central Pacific and Atlantic ocean basins (one sign) and the center of the Asian continent (opposite sign). Here we have a major east–west seesaw of mass with amplitudes of 10–20 mb. Negative anomalies reside over relatively warm surfaces (winter/ocean and summer/continent), while, conversely, the cold surfaces (winter/land and ocean/summer) have positive $p_*$ anomalies. The extremes occur in January and July with little lag behind the sun. The oceanic anomalies are large in magnitude but smaller in horizontal scale than the Eurasian center, which extends also into Saudi Arabia, Pakistan, India, and North Africa. The North American continent, while conforming to the general picture, plays a smaller role in the seasonal exchange.

We performed an empirical orthogonal function (EOF) analysis on the 12 pressure anomaly maps. All leading EOFs have time series associated with them (12 values only) that look very much like harmonics. The fields shown for January and July are representative of the first EOF, whose time series is a first harmonic of the seasonal cycle. The first EOF explains 82% of the variance, a very dominant signal. Indeed, January and July are very much each other's opposite. There is another much weaker first harmonic with 7% explained variance associated with the second EOF that peaks in the transition seasons, that is, three months out of phase with the time series of EOF 1. This second EOF is characterized by mass exchange between land and ocean in the subtropics. This mode is captured to some degree by the April and October maps, which are opposites to some extent. For instance, in April the oceanic subtropical highs are anomalously strong, while heat lows form over India/Pakistan and the southern United States, whereas the opposite occurs in October.

Some high- and low-latitude details in Fig. 1 are "explained" by higher-order EOFs (second and third

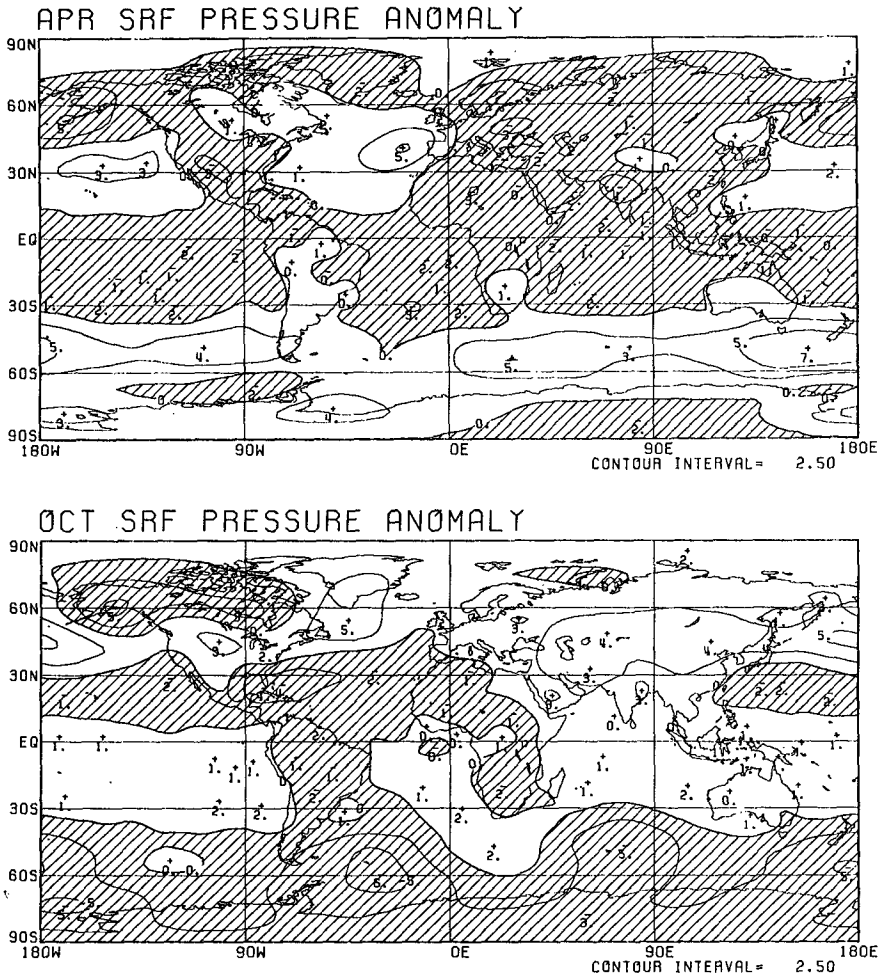


FIG. 1. (*Continued*)

harmonics) of, overall, very low variance. In the SH the land–sea exchange is small compared to the NH but nevertheless noteworthy with +6 mb anomalies in July over land. One can also see that high elevations have a seasonal cycle *opposite* to that of lower elevations; see for instance the Tibetan Plateau in Fig. 1. Finally, note that northwestern Canada and Alaska are more in tune with the ocean than with the landmasses.

When considering zonal averages, the dominance of the NH land–sea exchange is eliminated. The zonal mean $p_*$ anomalies in the model (not shown) match nature rather closely [see Fig. 3a in Trenberth et al.'s (1987) or Table 27 in Oort (1983)]. A negative $p_*$ anomaly appears to travel from south to north and back again in conjunction with the maximum in incoming solar radiation. At 25°N/S this anomaly reaches −2.5 mb but is less than 1 mb when crossing the equator. The swath of negative zonal mean $p_*$ anomalies underneath the sun is accompanied by two bands of positive $p_*$ anomalies on either side that move along north and south seasonally.

With only a few exceptions, the rule of thumb appears to be that relatively lower pressure is found over relatively warmer surfaces. This mode of operation is particularly clear in the NH, that is, high (low) pressure over land (ocean) in winter, and the reverse in summer. This behavior is in close agreement with the "thermal theory of pressure change" (Schmidt 1946; Austin 1951), at least qualitatively.

### *b. Divergent mass flux*

Figure 2 shows the 2D divergent mass fluxes. Although equivalent to showing $\partial p_*/\partial t$, which can be surmised by the reader from Fig. 1, the vector display in Fig. 2 gives not only a more vivid dynamic representation but also tells where the air comes from (is going to). In order to save space only April and October are shown. These are the transition months when the mass flux is largest. In both panels the longest vectors correspond to a velocity of about 3.5 mm $s^{-1}$. Remember that $\langle \mathbf{V} \rangle$ generally does not look like the sur-

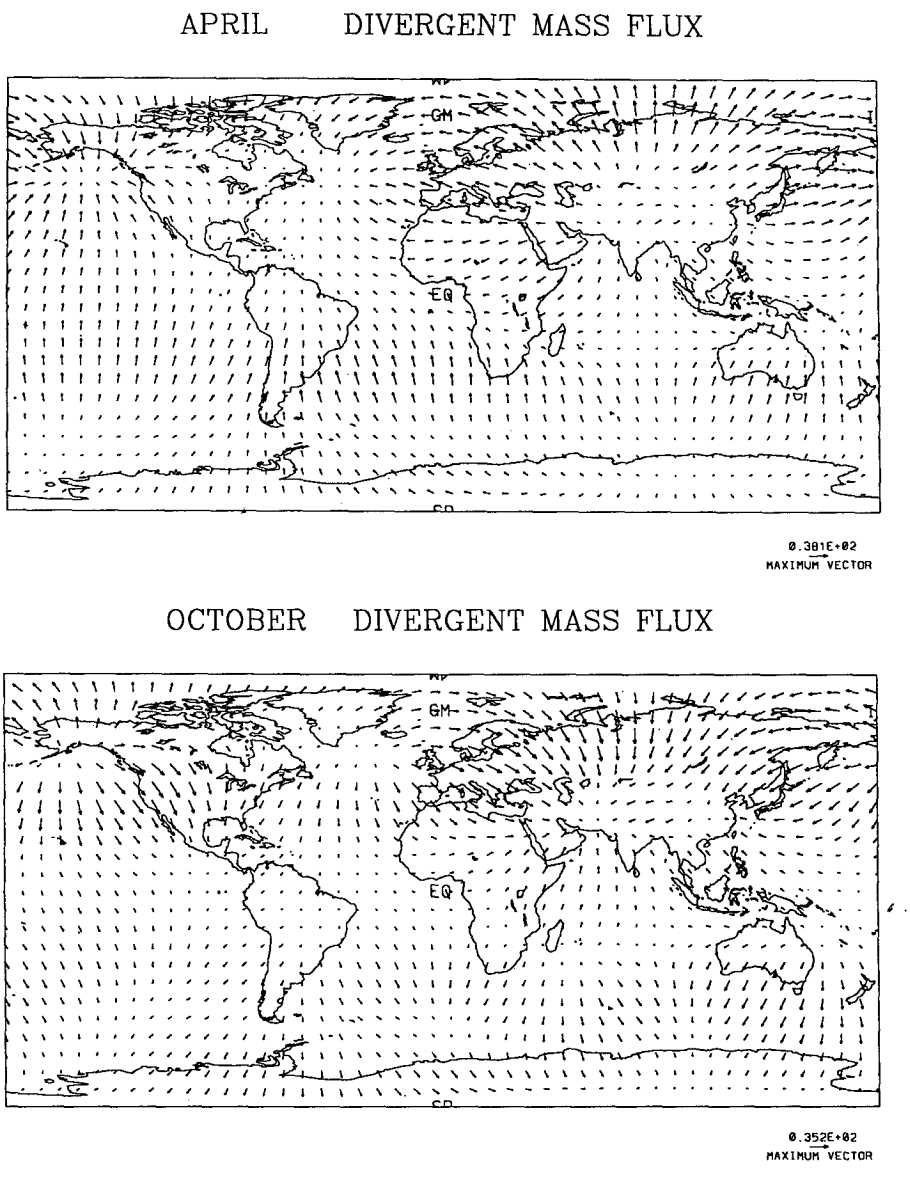


FIG. 2. The divergent mass flux in April and October. The length of the vector is proportional to the magnitude of the divergent mass flux. The maximum length (normalized) of the vector represents 3.8 and 3.5 mm $s^{-1}$, respectively.

face winds. In March and April mass residing over south-central Asia flows away in all directions but primarily into the area of the (wintertime) NH oceanic lows. Mass flows from Asia into the Pacific low from west to east, as well as across the pole. In April one can also see the primarily zonally symmetric meridional flow of mass from southern midlatitudes into the southern subtropics. In October and November one can see that, roughly, the opposite take place.

The scales at which mass is redistributed are very large but primarily intrahemispheric. The transport across the equator (see Fig. 2) is only a small part of the seasonal redistribution unless zonal averages are taken. Trenberth et al. (1987, Fig. 4) and Oort (1983, Fig. 39b) calculated the zonally averaged cross-equatorial mass flux from $p_*$ data. There is fair agreement between the model and their observational results.

## 4. Discussion

### *a. Sea level pressure and surface pressure*

One important advantage of the model over observations is that the former permits an exact bookkeeping of mass. Suppose the model output were provided in terms of sea level pressure. How much information

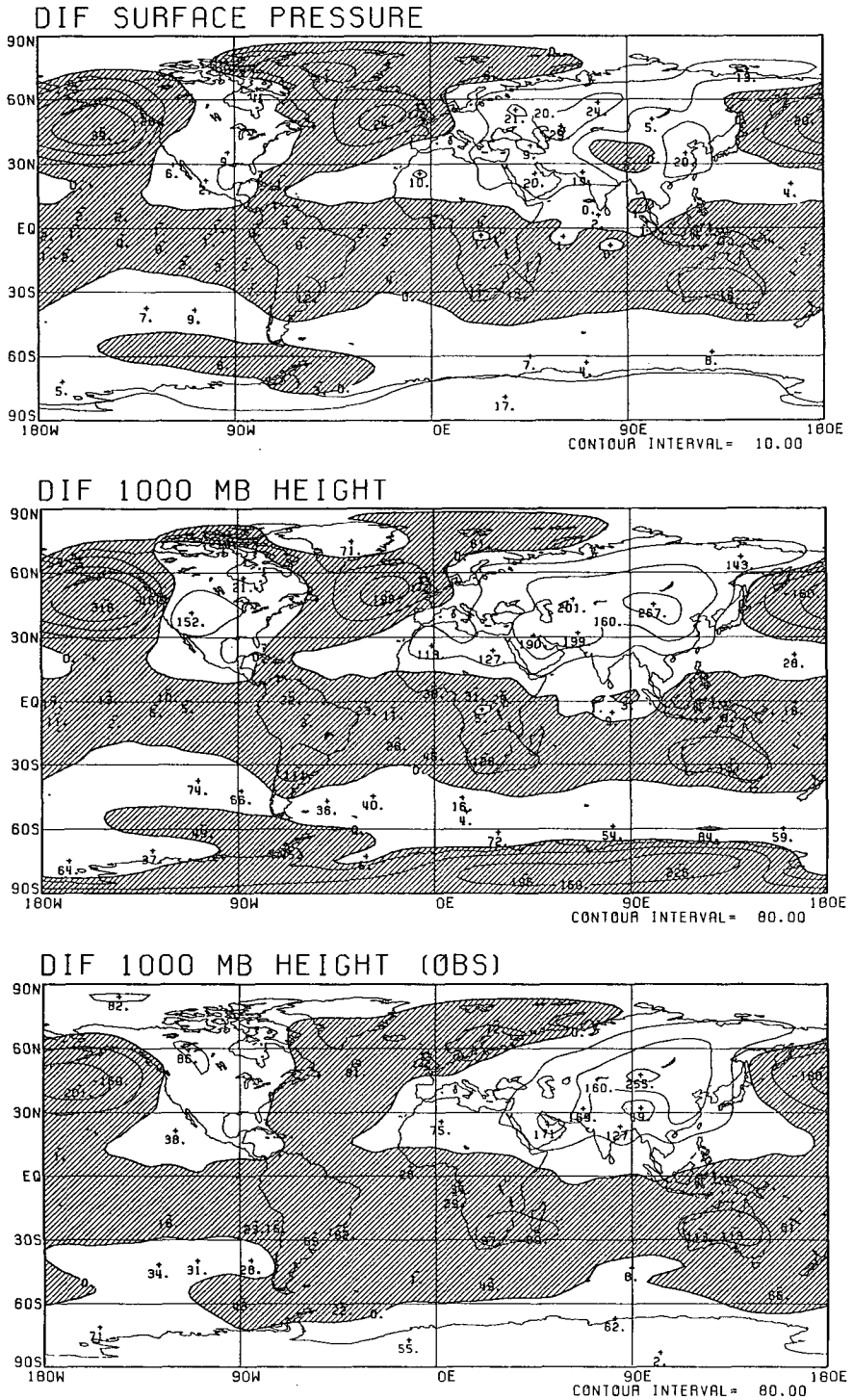


FIG. 3. January minus July difference in surface pressure (upper), in 1000-mb height (middle), and in *observed* 1000-mb height (bottom panel). Contours are 10 mb and 80 gpm. Negative values (i.e., July larger than January) are shaded.

would be lost (i.e., how much mass is fabricated/destroyed)? The answer can be judged from the upper two panels of Fig. 3. In this figure the model's January minus July difference is given for $p_*$ (top) and 1000-mb height (middle). The latter is obtained by standard postprocessing procedures (i.e., assuming a −6.5

K km$^{-1}$ lapse rate and integrating the hydrostatic equation downward). The contouring is almost identical, that is, 10 mb and 80 gpm, respectively. In areas without significant surface elevation, the two maps are virtually identical. Elsewhere, however, there are large differences; so much so that the annual cycles in sea level pressure over high terrain can be completely fictitious (Hsu and Wallace 1976) and opposite to the annual cycles in surface pressure. Significant inconsistencies are also seen at some lower elevations. Over Asia the true seasonal contrast in mass (top) in the model tends to be in the west and not in the central and eastern portions (middle panel) where the Siberian sea-level-pressure high resides in winter.

A reduction of $p_*$ to some standard level will always create or destroy mass. Considering (1), one can, however, leave the implied divergent mass flux intact as long as the time rate of change of pressure does not change when applying the reduction. From the previous paragraph it is clear that the time rates of change in surface and sea level pressure are very different over land. This implies rather different divergent mass fluxes, not just over land, but also over the oceans (not shown). For studies of the mass budget, the reduction method employed here (subtract the annual mean) or Oort's (1983) method are to be preferred over the far more common sea level pressure datasets. It is better yet to use the original surface pressure data.

The model's 1000-mb height January minus July difference (middle of Fig. 3) allows a comparison with the Climate Analysis Center's 10-year climatology (1978–88), based on twice-daily analyses (see lower panel of Fig. 3). The two 1000-mb height displays share the same surface to sea level pressure conversion. In areas without elevation the model seems qualitatively correct but has far too strong a seasonal contrast in the Pacific and Atlantic lows. The zonally symmetric mode at, and south of, the equator is more or less correct. Performance over land is hard to judge. Over Asia the model and observed 1000-mb heights are reasonably similar, implying probably the same degree of resemblance in $p_*$.

### b. *Water mass budget*

The mass budget just described is governed in the model by Eq. (1). The model has, however, a second distinct mass budget, for water in the atmosphere, based on its continuity equation:

$$\partial \rho_v / \partial t = -\nabla \cdot (\rho_v \mathbf{V}) + S, \qquad (4)$$

where $\rho_v$ is the water vapor density and $S$ is a sink/source term. Upon vertical integration (4) becomes

$$\partial e_* / \partial t = -g\nabla \cdot \mathbf{M}_v - g(P - E), \qquad (5)$$

where $e_*/g$ is the mass of the water in the vertical column (i.e., the precipitable water), $\mathbf{M}_v$ is the vertically integrated water mass flux, and $(P - E)$ is the difference between precipitation and evaporation. (Note that $e_*$ is not Dalton's partial vapor pressure.) In the model (1) and (5) are kept separately, but in nature dry air and water in the air are coupled (additive):

$$\partial p_* / \partial t = -g\nabla \cdot \mathbf{M} - g(P - E), \qquad (6)$$

where $p_* - e_*$ is the mass due to dry air and $\mathbf{M}$ is the divergent total mass flux due to moist and dry air. Equation (1) was, erroneously, intended to hold for total mass, and the model integrations are started from observed total surface pressure. We propose that the NMC (and all other) models should be using (6) instead of (1).

Equation (6) can also be written as

$$\partial (p_* - e_*)/\partial t + \partial e_*/\partial t = -g\nabla \cdot \mathbf{M}_{\text{dry}} - g\nabla \cdot \mathbf{M}_v - g(P - E), \qquad (6a)$$

where $\mathbf{M}_{\text{dry}}$ is the mass flux due to dry air alone. Subtracting (5) from (6a) results in the conservation equation of dry air.

The difference between the current NMC model (and most, if not all other models) and nature is, roughly, as follows. When water evaporates from the surface into the model atmosphere, or when rain falls, the hydrostatic surface pressure is not changed; only the virtual temperature changes. This means that total mass is conserved, but the mass of dry air is not (i.e., dry air is destroyed or created to conserve total mass). In nature dry air is conserved and the surface pressure, of course, changes as a result of sinks and sources of water. While revising the manuscript, it was brought to our attention that the same change in the continuity equation has been proposed by Qiu et al. (1991) and Geleyn et al. (1991) for modeling purposes, and by Trenberth (1991) for diagnostic studies. We will report on runs with the correct continuity equation in the near future.

From maps of $(P - E)$ in the model (not shown) one can see that the subtropical oceans are (or ought to have been) a substantial source of mass, on the order of 10–30 mb per month. The pattern is similar in summer and winter. The sinks are the mid- and higher latitudes, as well as areas of concentrated tropical convection. It appears, therefore, that we left out the largest term from the continuity equation (6) by using (1). Assuming that $(P - E)$ is primarily balanced by $g\nabla \cdot \mathbf{M}_v$ implies divergent water mass fluxes on the order of centimeters per second, that is, much larger than the ones shown in Fig. 2, and of a rather different pattern. Moreover, $\mathbf{M}_v$ has a very large annual mean component. A complete assessment of the impact of using (6) instead of (1) can only be determined by rewriting the equations and model code and repeating the experiment. We would then be able to show separately the divergent mass fluxes due to dry air and water and how they balance to produce rather small changes in $p_*$ over the course of the annual cycle.

It is conceivable that the coupling of dry air and water mass [i.e., the use of Eq. (6)] is important also on time scales much shorter than the annual. Considering the magnitude of $(P - E)$ and the smallness of observed surface pressure changes, this must certainly be the case in the tropics. In midlatitude day-to-day weather the contribution of water sources/sinks pressure tendencies would appear to be quite small and has not even been mentioned in otherwise exhaustive studies (Schmidt 1946) on the mechanism of surface pressure change.

Globally averaged $p_*$ can only change due to the $(P - E)$ imbalance. Trenberth (1981) and Christy et al. (1989) estimate that the observed surface pressure in July is, for that reason, about 0.4 mb higher than in January. This feature basically reflects the annual cycle in atmospheric temperature and the atmosphere's capacity to hold water. In the model both $P$ and $E$ have a well-defined and rather similar annual cycle (see Fig. 4), $E$ having the larger amplitude. As long as $E > P$ the model's global mean surface pressure ought to have increased, but as we have noted it was not permitted to do so. From minimum (January/February) to maximum (August) the pressure should have increased by about 0.3 mb, a bit less than that found by Trenberth (1981). Compared to observations (Brutsaert 1984; Elliott et al. 1991), the model, which is too cold, appears to hold too little precipitable water (21 versus 25–27 mm) and has a proportionally smaller annual cycle in $e_*$. (The discrepancy is perhaps even larger given that the observations of humidity are not integrated to the top of the atmosphere, but only to 500 mb, or, in other studies, to the level where the radiosonde balloon bursts.)

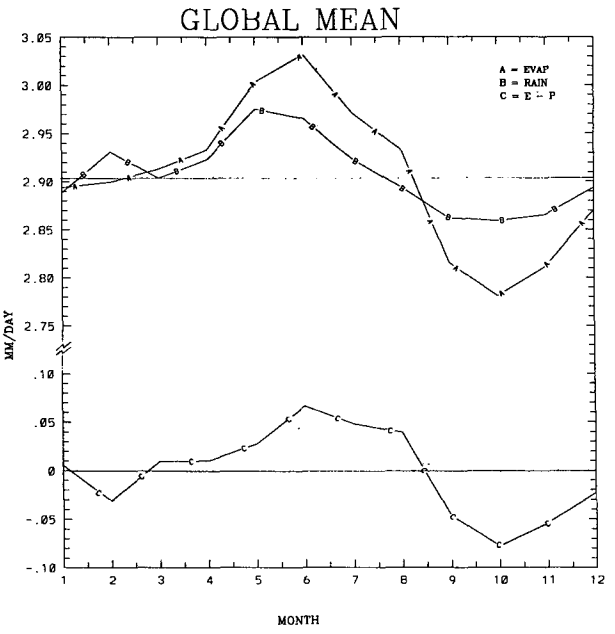


FIG. 4. Global mean evaporation ($E$), precipitation ($P$), and ($E - P$) as a function of month. Units are millimeters per day. The straight lines represent global and annual values.

## 5. Conclusions

In this paper we have presented the seasonal redistribution of mass as it occurs in a 10-year run of the NMC MRF model. Qualitatively, the model reproduces the observed annual cycle in surface pressure reasonably well, except south of 30°S where the model appears to be poor (see Fig. 3). Relatively lower pressures are generally found over surfaces that are warm relative to their environment. The seasonal exchanges take place in two primary modes, which appear realistic. The first is an intrahemispheric redistribution involving the NH midlatitude oceanic basins and the Asian continent. The second is a triplet of zonally symmetric pressure anomalies near the equator and in the SH. [Coincidentally or not, these "centers of action" for the seasonal redistribution of mass are more or less the same as the ones involved in interannual variability in $p_*$ (Christy et al. 1989).] The NH pattern is "overdone" by the model by some 50%–100%, that is, the seasonal contrast is much too large, but qualitatively, the model behaves very much like the observations as reported by Gordon (1953), Hsu and Wallace (1976), and Trenberth (1981), and described long before (see older references in these papers).

The classical literature on monsoons naturally focuses on the tropics and subtropics. Accepted northernmost boundaries of the Asian summer monsoon are about 40°N over East Asia. There have been some attempts by climatologists (Lamb 1972) to attribute the increase in westerly circulation types over Western Europe late in June to a monsoon. From the point of view of mass, most of the seasonal rearrangements do in fact take place in NH midlatitudes.

With respect to observations of the annual cycle in sea level pressure, it has been noted in classical texts (Schmidt 1946; Austin 1951; Wallace and Hobbs 1976) that the so-called thermal theory of pressure change applies reasonably well. This means that the relatively higher(lower) pressure is to be expected over the relatively colder(warmer) surfaces. ("Relative" refers to other locations at the same time.) The NMC MRF model appears to behave according to the same macrophysical law, although precision is lacking. We speculate that part of the observed interannual variability, particularly the Southern Oscillation, is governed by the same principle, that is, lower(higher) than normal $p_*$ over warmer(colder) than normal sea surface temperature.

We have found at least one potentially serious problem in the model simulation. We conclude that the continuity equations for atmospheric water and total air ought to be consistent such that dry mass is conserved, and the tendencies in total pressure (at the sur-

face as well as aloft) include a contribution from the net water mass input (precipitation minus evaporation). To this end, we propose to change the continuity equation used in the model so far. This would introduce a mechanism for atmospheric circulation to be driven by water mass sources and sinks, for which we propose the name "water mass forcing." This aspect is currently missing in the MRF model (and most if not all other models used for similar purposes). In present models the hydrological cycle is important for latent heat release, clouds, and radiation. Otherwise, water is advected as a passive tracer of no direct consequence to the mass field. The inclusion of water mass forcing adds urgency to getting the correct $(P - E)$ distributions in models. Use of the correct continuity equation would also allow us to display the divergent mass fluxes of dry air and water separately. These separate mass fluxes are likely to be much larger than the ones shown in Fig. 2.

*Acknowledgments.* The authors are grateful for the comments received from J. Anderson, A. G. Barnston, M. Chelliah, J. D. Murphree, Å. Johansson, D. J. Gaffen, and W. Elliott. We are particularly grateful to Dr. A. H. Oort for sharing with us an unpublished manuscript by J.-P. Huot and for giving good advice.

## REFERENCES

Austin, J. M., 1951: Mechanism of pressure change. *Compendium of Meteorology,* T. F. Malone, Ed., Amer. Meteor. Soc., 630–638.

Boer, G. J., 1986: A comparison of mass and energy budgets from two FGGE datasets and a GCM. *Mon. Wea. Rev.,* **114,** 885–902.

Brutsaert, W., 1984: *Evaporation into the Atmosphere.* Reidel, 299 pp.

Christy, J. R., K. E. Trenberth, and J. R. Anderson, 1989: Large-scale redistribution of atmospheric mass. *J. Climate,* **2,** 137–148.

Elliott, W. P., M. E. Smith, and J. K. Angell, 1991: Monitoring tropospheric water vapor changes using radiosonde data. *Greenhouse-Gas-Induced Climate Change: A Critical Appraisal of Simulations and Observations,* M. E. Schlesinger, Ed., Elsevier, 311–327.

Geleyn, J-F., M. Rochas, and Ph. Courtier, 1991: Special features of the unparameterized set of equations for the "ARPEGE" NWP system at DMN. *Proc. of the Ninth Conf. on Numerical Weather Prediction,* Denver, Amer. Meteor. Soc., 231–233.

Gordon, A. H., 1953: Seasonal changes in the mean pressure distribution over the world and some inferences about the general circulation. *Bull. Amer. Meteor. Soc.,* **34,** 357–367.

Hsu, C.-P. F., and J. M. Wallace, 1976: The global distribution of the annual and semiannual cycles in sea level pressure. *Mon. Wea. Rev.,* **104,** 1597–1601.

Lamb, H. H., 1972: *Climate: Present, Past and Future.* Vol. 1. *Fundamentals and Climate Now.* Methuen, 613.

Murphree, J. T., and H. M. van den Dool, 1988: Calculating tropical winds from time mean sea level pressure fields. *J. Atmos. Sci.,* **45,** 3269–3282.

Oort, A. H., 1983: Global Atmospheric Circulation Statistics, 1953–1973. NOAA Prof. Paper 14.

Qiu, Q-J., J-W. Bao, and Q. Xiu, 1991: The significance of mass sink due to precipitation. *Proc. of the Ninth Conf. on Numerical Weather Prediction,* Denver, Amer. Meteor. Soc., 364–365.

Ramage, C. S., 1971: *Monsoon Meteorology.* Academic Press, 296 pp.

Schmidt, F. H., 1946: On the causes of pressure variations at the ground. *Meded. Verh., Ser B,* I **4,** 38 pp.

Trenberth, K. E., 1981: Seasonal variations in global sea level pressure and the total mass of the atmosphere. *J. Geophys. Res.,* **86,** 538–5246.

——, 1991: Climate diagnostics from global analyses: Conservation of mass in ECMWF analysis. *J. Climate,* **4,** 707–722.

——, J. R. Christy, and J. G. Olson, 1987: Global atmospheric mass, surface pressure, and water vapor variations. *J. Geophys. Res.,* **92,** 14 815–14 826.

Wallace, J. M., and P. V. Hobbs, 1977: *Atmospheric Science. An Introductory Survey.* Academic Press, 467 pp.